

Combination of Magic-Echo and Single-Point Imaging Techniques for Solid-State MRI

Z. Fang and D. Hoepfel

Fachbereich Mechatronik und Naturwissenschaften, Hochschule für Technik, Karlsruhe, Germany

Received October, 3 2001; revised November, 19 2001

Abstract. Due to reduced molecular motion the transverse relaxation time T_2 in solid materials is typically shorter by a factor of 10^3 to 10^5 in comparison to those in liquids, resulting in a large intrinsic nuclear magnetic resonance line-width that can be well above 20 kHz. Therefore high-resolution solid-state magnetic resonance imaging requires either very strong gradients or special line-narrowing techniques. Single-point imaging (SPI) is a successful pure phase encoding sequence in imaging soft-solid materials; however, when used to study rigid solid materials it still suffers from a very long acquisition time and large gradients. On the other hand, magic echo is a technique that can be used to effectively refocus dipolar interaction, thus achieving a line narrowing. Therefore, the aim of this work is to improve the signal intensity with the combination of the magic echo technique and the SPI sequence. In this paper first applications and a comparison of the SPI sequence with a combination of the magic echo and the SPI sequence to image structures of solid-state materials are presented.

1 Introduction

Due to reduced molecular motion the transverse relaxation time T_2 in solid materials is typically shorter by a factor of 10^3 to 10^5 in comparison to those in liquids, resulting in a large intrinsic nuclear magnetic resonance (NMR) line-width that can be well above 20 kHz [1]. In the case of solid-state magnetic resonance imaging (MRI), the transverse magnetization M_x/M_y decays so fast that only a small amount is left before any conventional MRI sequences can be successfully applied, therefore the achievable spatial resolution and the signal-to-noise ratio is strongly degraded. Two classes of methods are commonly used to do solid-state MRI: using large gradients and using line-narrowing techniques. The class of imaging methods characterized with large gradients includes stray-field imaging (STRAFI) [2], pure phase encoding imaging such as single-point imaging (SPI) [3], and multiquantum imaging [4]. The class of imaging methods characterized with line-narrowing techniques includes magic-angle spinning (MAS) imaging [5], magic-angle rotating-frame imaging [6], multipulse line narrowing imaging [7, 8], and magic echo phase-encoding imaging [9, 10]. Most of these

solid-state MRI methods require additional hardware, therefore are difficult to realize with standard MRI devices and have limited applications. From an experimental point of view, pure phase encoding are the most suitable methods to do solid-state imaging of abundant nuclei ^1H . SPI is a successful pure phase encoding sequence in imaging soft-solid materials. However, the limiting disadvantage of SPI is a very long acquisition time. To reduce the acquisition time, an improved version of SPI, single-point ramped imaging with T_1 enhancement (SPRITE), was proposed by Balcom [11]. SPI/SPRITE have been successfully applied to study various materials with short transverse relaxation times, such as cement [12–14], zeolite [15] and gas [16]. However, in most rigid solid materials the dipolar interaction is so strong that the transverse magnetization decays to noise level in 20 μs or even less. High-resolution imaging of rigid solids with SPI/SPRITE sequences still suffers from very strong gradients and the low signal-to-noise ratio. In this case the strategy to extend the decaying time of transverse magnetization is the use of different line-narrowing techniques, such as solid-echo [17] and magic echo [18] sequences. In this paper results of the SPI sequence combined with the magic echo SPI sequence to study structures of solid-state materials are presented.

2 Materials and Methods

Single-point imaging is a three-dimensional (3-D) pure phase encoding method, a single data point in the k -space is acquired with a minimum phase encoding time after each broadband, small flip angle (typically 10°) radio-frequency (RF) excitation pulse. The SPI sequence is shown in Fig. 1. The signal intensity S from any point in an SPI image is related to local proton density, ρ , by Eq. (1) where the pulse flip angle is θ , the phase encoding time is t_p and the repetition time is T_R [11]:

$$S = \rho \exp\left(-\frac{t_p}{T_2^*}\right) \left[\frac{1 - \exp(-T_R/T_1)}{1 - \cos\theta \exp(-T_R/T_1)} \right] \sin\theta. \quad (1)$$

The term in square brackets represents steady-state longitudinal magnetization established through a succession of excitation pulses where we assume transverse magnetization is completely dephased between pulses. This term suggests the possibility of introducing T_1 contrast into the image by employing large flip angle pulses with repetition times in the order of T_1 . The shorter T_1 of many systems of interest further suggests that rapid pulsing should permit rapid k -space traversal. The main advantages of the SPI method are: no requirement of additional hardware, ultrashort phase encoding time, no chemical shift and susceptibility artifacts, insensitivity to B_0 field inhomogeneity. The limiting disadvantage is a long acquisition time, which is due to the fact that only one data point is acquired after each excitation pulse.

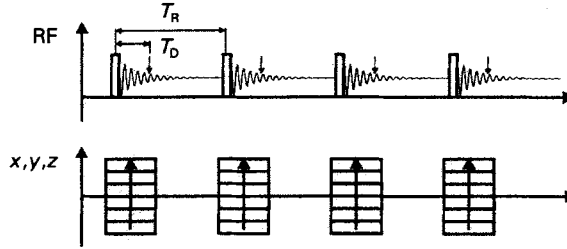


Fig. 1. SPI pulse sequence. x, y, z represent three gradient directions, T_R is the repetition time and T_D is the phase-encoding time. Only one data point is acquired after each small flip angle excitation pulse (normally about 10°).

Magic echo is generated from transverse magnetization with magic sandwich pulses that are shown in Fig. 2 [9]. The excitation pulse 90_x produces coherences evolving during a time period of τ . The time reversal of the evolution in the presence of the spin interactions takes place as a consequence of the magic sandwich $90_y-\alpha_x-\alpha_x-90_y$. This composite pulse has a total length of 4τ . After another interval τ' , which ideally is identical to τ , the magic echo is created. In this sequence the $90_{\pm x, y}$ pulses are assumed to be “ideally hard”, i.e., the conditions $\omega_1 = \gamma B_1 \gg \gamma G_z d_z$ and $\omega_1 \gg \gamma B_{loc}$ are fulfilled, this condition is also termed “ δ pulse limit”. In this case the whole spectrum and the whole sample is excited homogeneously. Here the dimension of the sample in z direction is d_z , the gradient strength along the z direction is G_z , the local field is B_{loc} , the amplitude of the RF field is B_1 , and the gyromagnetic ratio of ^1H is γ . The nominal pulse angle α of the burst pulse is determined by the pulse length 2τ , i.e., $\alpha = 2\omega_1\tau$. These burst pulses are assumed to fulfil the condition $\omega_1 \gg \gamma B_{loc}$ but not necessarily $\omega_1 \gg \gamma G_z d_z$. During the burst pulses the dipolar interaction and the local off-resonance effect produced by the field gradient have to be taken into account. Unlike a 90° refocusing pulse in the solid echo sequence, the magic sandwich

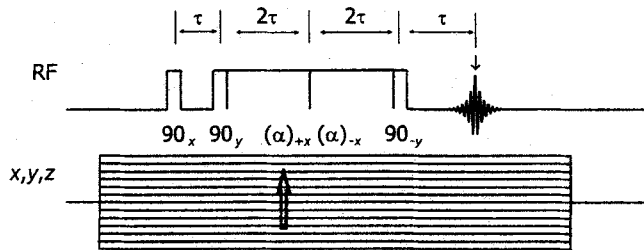


Fig. 2. Magic-echo SPI pulse sequence. x, y, z , represent three gradient directions. All $90_{\pm x, y}$ pulses are hard δ pulses, the dephasing time of the transverse magnetization is τ . The magic sandwich consists of four pulses with a total length 4τ . $90_y-\alpha_x-\alpha_x-90_y$, during which dipolar interaction is refocused. The nominal flip angle of the burst pulse is decided by $\alpha = 2\tau\gamma B_1$, B_1 is the RF field strength. Magic echo appears another τ after the magic sandwich.

is capable of refocusing magnetization, which decays under the dipole-dipole interaction not only between just two spins $1/2$ but also among many spins. Another feature of magic sandwich is that single-quantum coherences can be refocused even after delays as long as the transverse relaxation times, thus gradients can be switched on and off during these delays. In magic echo imaging the amplitude of the gradient pulses applied during the echo time is varied in a systematic way to cover k -space, so that phase encoding of the space information is realized. If the gradients cannot be switched on and off sufficiently rapidly, they can be left on during the magic sandwich as is the case in our laboratory. However, this will cause mirror artifacts in the final image.

In our laboratory SPI and the magic echo SPI sequences are used to do 2- and 3-D imaging of various solid-state materials, including Lego blocks, low-water-content chocolates, phantoms made from lupolen particles and glass fiber filled polypropylene samples. The Lego SPI experiments were carried out on a 0.35 T Bruker electro-magnet system located in the University of Applied Sciences in Karlsruhe, equipped with 200 mT/m active-shielding gradients which can be switched in ca. 600 μ s and a 200 W RF amplifier. All other experiments were made on a 4.7 T Bruker AVANCE spectrometer located in the University of Karlsruhe, equipped with 1 T/m gradients with 100 μ s switching on/off time and a 200 W RF amplifier. Some photos of the samples we measured are shown in Fig. 3. The Lego block is a normal Lego piece bought from a children toy-shop, its dimension is 24 by 12 by 16 mm; the Milka Luflee chocolate sample is from Kraft Co. in Munich with a dimension of 12.5 by 14.5 by 21 mm, and it has been naturally dried under room temperature for several weeks without any packing, so that the water (moisture) content is believed to be much lower than that in normal chocolate samples; the lupolen phantom sample is made from three packed lupolen particles of BASF Co., each with a size of 5 mm in diameter

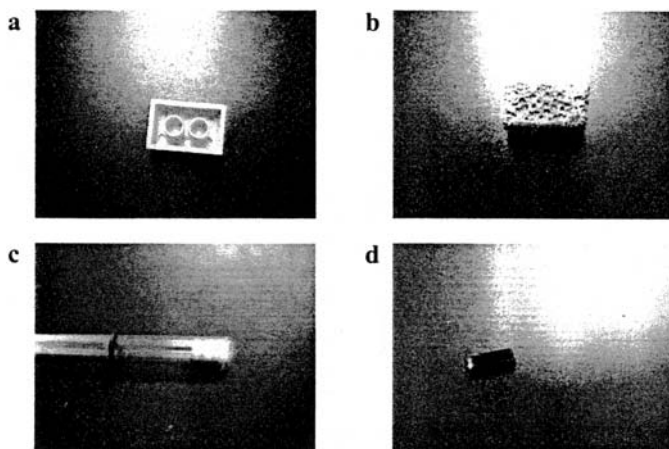


Fig. 3. Photos of the samples as described in the text: a a Lego block, b a Milka Luflee chocolate piece, c lupolen phantom, d glass fiber filled polypropylene sample.

and 2 mm in height. The glass fiber filled polypropylene sample is provided by Fraunhofer Institute for Chemical Technology in Pfinztal, Germany, in a cylinder form with a diameter of 5 mm and a height of 5 mm, the imbedded glass-fiber bundle is about 1.5 mm in diameter.

3 Results and Discussions

Figure 4 shows a surface reconstructed SPI image of a Lego block made on a 0.35 T system, having a resolution of $625 \mu\text{m}/\text{pixel}$ in all three spatial directions. The total experimental time was about 3 h. With this 0.35 T electro-magnet system, the signal-to-noise ratio and the achievable resolution is mainly limited by the low field strength B_0 . Another limiting factor is the long-time thermal stability of the water-cooled electro-magnet system. Because SPI method normally requires long experimental time, an SPI experiment made on a superconductive magnet system will perform better.

Figure 5 shows a 3-D reconstructed SPI image of a low-water-content chocolate sample measured on the 4.7 T system. In this case the achieved resolution is $176 \mu\text{m}/\text{pixel}$ in x, y directions and $352 \mu\text{m}/\text{pixel}$ in z direction, and the total acquisition time is about 19 h. The initial motivation of this experiment is to study the distribution of pores in this chocolate. On the image the bright areas represent the chocolate powder with bound water or fat, the dark areas are assumed to be void space. The distribution of pores as well as the porosity can be calculated from the image data, the accuracy of the porosity calculation is directly dependent on the signal-to-noise ratio of the experiment. With this kind of low-water-content chocolate sample we also tried to use the conventional spin echo Fourier imaging sequence; however, the obtained signal intensity was too weak to be used for further evaluation.

Figure 6 shows two 2-D images of the lupolen phantom obtained with the SPI sequence and the magic echo SPI sequence. With the magic echo sequence

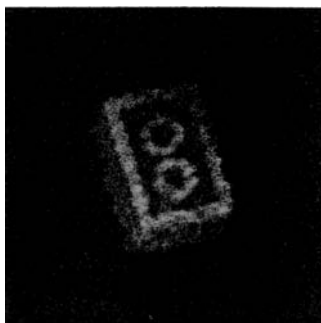


Fig. 4. 2-D surface reconstructed SPI image of the Lego block made on a 0.35 T electro-magnet system. Field of view (FOV) is 4.0 by 4.0 by 4.0 cm, resolution is 625 by 625 by 625 $\mu\text{m}/\text{pixel}$, total experimental time is 17 h.

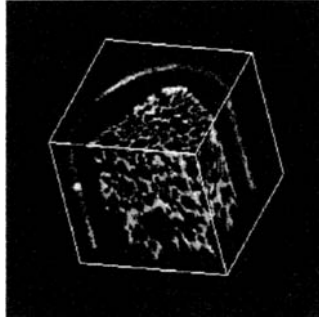


Fig. 5. 3-D reconstructed SPI image of the Milka Luflee chocolate sample made on a 4.7 T Bruker microimaging system. FOV is 2.2 by 2.2 by 2.2 cm, resolution is 176 by 176 by 352 $\mu\text{m}/\text{pixel}$, total experimental time is 19 h.

the line-narrowing effect leads to an effective transversal magnetization relaxation time T_2^* of ca. 250 μs compared to ca. 40 μs of intrinsic T_2^* . The images are 2-D along the z direction, projected onto the other direction without slice selection. The achieved resolution and total experimental time are 375 $\mu\text{m}/\text{pixel}$ in 5 min for the SPI sequence and 390 $\mu\text{m}/\text{pixel}$ in 27 min for the magic echo SPI sequence. The relatively long acquisition time of the magic echo SPI sequence compared to the normal SPI sequence is due to the fact that a 90° excitation pulse and a long repetition time (longer than T_1) are used for the full recovery of the longitudinal magnetization. Other important acquisition parameters are: for the SPI sequence, the phase encoding time τ is 45 μs , repetition time is 10 ms and the number of averages is 32; for the magic echo SPI sequence, the dephasing time τ is 60 μs , repetition time is 400 ms, the number of averages is 4

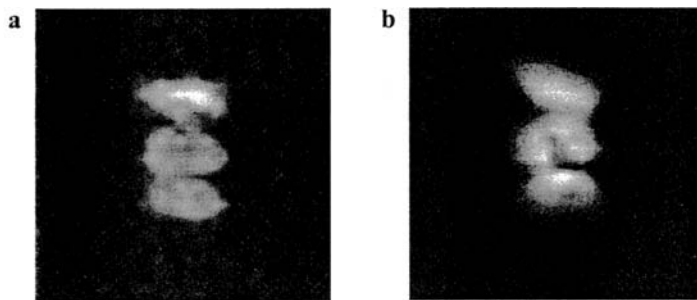


Fig. 6. 2-D images of the lupolen phantom made on a 4.7 T Bruker microimaging system. The images are acquired along the z direction of the Bruker 5 mm microimaging birdcage probe and projected onto the third direction without slice selection. **a** Normal SPI sequence, with 45 μs phase encoding time, 10 ms repetition time and 32 scans. The resolution is about 375 $\mu\text{m}/\text{pixel}$, and total acquisition time is about 5 min; **b** magic echo SPI sequence, with 60 μs dephasing time τ , 400 ms repetition time and 4 scans, and B_1 for the burst pulse is about 10 G. The resolution is about 390 μm , the total acquisition time is about 27 min.

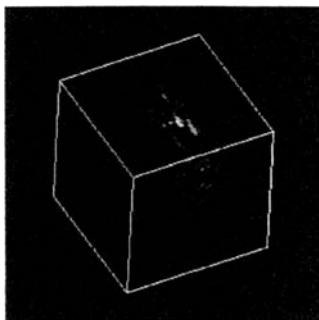


Fig. 7. 3-D reconstructed magic echo SPI image of the glass fiber filled polypropylene. The sample made on a 4.7 T Bruker microimaging system. Resolution is about $180\ \mu\text{m}/\text{pixel}$, total experimental time is about 43 h. Artifacts are present at the center of the 3-D image. The bright area represents the polypropylene shell, and the dark area is the imbedded glass fibre bundle.

and the B_1 field strength for the two RF burst pulses is about 1 mT. These two images present a comparison of the two applied sequences, a clear improvement in the signal-to-noise ratio is achieved with the magic echo technique, although only 4 scans are accumulated compared to 32 scans in the normal SPI sequence. However, in the magic echo SPI sequence the total acquisition time is longer than that of the normal SPI sequence due to the fact that a 90° pulse is used for spin excitation instead of a small flip angle excitation pulse. Further work is continued in our group to investigate the possibility to use a small flip angle (steady-state excitation) with the magic echo SPI sequence.

Figure 7 shows a 3-D reconstructed image of the glass fiber filled polypropylene product in a 5 mm diameter cylinder form, which just fits in the Bruker 5 mm birdcage microimaging probe of the 4.7 T system. The transversal magnetization relaxation time T_2^* of the sample is estimated at about $40\ \mu\text{s}$. The achieved resolution is about $180\ \mu\text{m}/\text{pixel}$ and the total experimental time is about 43 h. Although the image is rather noisy and some artifacts are present in the center, the structure consisting of an outer polypropylene shell and a central glass fiber bundle can be clearly identified. Great interest from the chemical industry is expressed for a similar product that has an (ideally) evenly distributed glass fiber network in the cross section, and the interest is the relation between the distribution of the glass fibers and the mechanical performance of the products. In this case, the diameter of the glass fiber (or thin fiber bundle) is in the range of 20–50 μm which cannot be resolved with the currently used magic echo SPI sequence.

4 Summary

The experiments described above show some preliminary results of the application of solid-state MRI on standard equipment by using SPI in combination with magic echo SPI sequences. Clearly, the resolution (limited by the signal-to-noise

ratio) is not sufficient for many practical high-resolution applications, and the total experimental time is too long. To reduce the total acquisition time, two approaches are: using small flip angle steady-state excitation with magic echo SPI sequence; using spin-locking slice selection [19] technique with magic echo SPI sequence. In our group work along this direction is continuing.

Acknowledgements

We thank Dr. G. Guthausen from the DFG NMR laboratory at the University of Karlsruhe for her help in programming the magic echo SPI sequence and in the performing the experiments; Dr. A. Geissler from Fraunhofer Institute for Chemical Technology in Pfinztal, Germany, for kindly providing the Lupolen and the glass fiber filled samples. Finally, we thank DFG (German Research Foundation) for the financial support.

References

1. Blümich B.: *NMR Imaging of Materials*. Oxford: Clarendon Press 2000.
2. Samoilenko A.A., Artemov D.Yu., Sibel'dina L.A.: *JETP Lett.* **47**, 417–419 (1988)
3. Emid S., Carygton J.H.N.: *Physica B* **128**, 81–83 (1985)
4. Garroway A.N., Baum J., Munowitz M.G., Pines A.: *J. Magn. Reson.* **60**, 337–341 (1984)
5. Cory D.F., Os J.W.M., Veeman W.S.: *J. Magn. Reson.* **76**, 543 (1988)
6. Maraviglia Luca B.F., Simone B.C., Luger N. in: *Encyclopedia of NMR* (Grant D.M., Harris R.K., eds.), p. 2715. New York: Wiley 1996.
7. Chingas G.C., Miller J.B., Garroway A.N.: *J. Magn. Reson.* **66**, 530–535 (1986)
8. Cory D.G., Miller J.B., Garroway A.N.: *J. Magn. Reson.* **90**, 205–213 (1990)
9. Demco D.E., Hafner S., Kimmich R.: *J. Magn. Reson.* **96**, 307–332 (1992)
10. Matsui S.: *Chem. Phys. Lett.* **179**, 87–190 (1991)
11. Balcom B.J. in: *Spatially Resolved Magnetic Resonance: Methods, Materials, Medicine, Biology, Rheology, Geology, Ecology, Hardware* (Blümli P., Blümich B., Botto R.E., Fukushima E., eds.). Weinheim: Wiley-VCH 1998.
12. Beyea S.D., Balcom B.J., Bremner T.W., Prado P.J., Cross A.R., Armstrong R.L., Grattan-Bellew P.E.: *Solid State NMR* **13**, 93–100 (1998)
13. Prado P.J., Balcom B.J., Beyea S.D., Armstrong R.L., Bremner T.W., Grattan-Bellew P.E.: *Magn. Reson. Imaging* **16**, 521–523 (1998)
14. Beyea S.D., Balcom B.J., Bremner T.W., Prado P.J., Green D.P., Armstrong R.L., Grattan-Bellew P.E.: *Cem. Concr. Res.* **28**, 453–463 (1998)
15. Prado P.J., Balcom B.J., Jama M.: *J. Magn. Reson.* **137**, 59–64 (1999)
16. Prado P.J., Balcom B.J., Mastikhin I.V., Kennedy C.B., Armstrong R.L., Logan A.: *J. Magn. Reson.* **137**, 324–332 (1999)
17. McDonald P.J., Attard J.J., Taylor D.G.: *J. Magn. Reson.* **72**, 224–229 (1987)
18. Rhim W.-K., Pines A., Waugh J.S.: *Phys. Rev. B* **3**, 684–696 (1971)
19. Demco D.E., Kimmich R., Hafner S., Weber H.-W.: *J. Magn. Reson.* **94**, 317–332 (1991)

Authors' address: Dieter Hoepfel, FB Mechatronik und Naturwissenschaften, Hochschule für Technik, Moltkestrasse 30, 76133 Karlsruhe, Germany